European Extremely Large Telescope Site Characterization I: Overview
Author(s): Jean Vernin, Casiana Muñoz-Tuñón, Marc Sarazin, Héctor Vazquez Ramió, Antonia M. Varela, Hervé Trinquet, José Miguel Delgado, Jesús Jiménez Fuensalida, Marcos Reyes, Abdelmajid Benhida, Zouhair Benkhaldoun, Diego García Lambas, Youssef Hach, M. Lazrek, Gianluca Lombardi, Julio Navarrete, Pablo Recabarren, Victor Renzi, Mohammed Sabil, Rubén Vrech
Reviewed work(s):
Source: *Publications of the Astronomical Society of the Pacific*, Vol. 123, No. 909 (November 2011), pp. 1334-1346
Published by: The University of Chicago Press on behalf of the Astronomical Society of the Pacific
Stable URL: http://www.jstor.org/stable/10.1086/662995
Accessed: 23/11/2011 07:43

PUBLICATIONS OF THE ASTRONOMICAL SOCIETY OF THE PACIFIC, **123**:1334–1346, 2011 November

European Extremely Large Telescope Site Characterization I: Overview

JEAN VERNIN,[1] CASIANA MUÑOZ-TUÑÓN,[2,3] MARC SARAZIN,[4] HÉCTOR VAZQUEZ RAMIÓ,[2]
ANTONIA M. VARELA, [2,3] HERVÉ TRINQUET,[1] JOSÉ MIGUEL DELGADO,[2] JESÚS JIMÉNEZ FUENSALIDA, [2,3]
MARCOS REYES,[2] ABDELMAJID BENHIDA,[5,6] ZOUHAIR BENKHALDOUN,[5] DIEGO GARCÍA LAMBAS,[7]
YOUSSEF HACH,[5] M. LAZREK,[5] GIANLUCA LOMBARDI,[4]
JULIO NAVARRETE,[4] PABLO RECABARREN,[7] VICTOR RENZI,[7]
MOHAMMED SABIL,[5] AND RUBÉN VRECH[7]

Received 2011 July 14; accepted 2011 September 27; published 2011 November 1

ABSTRACT. The site for the future European Extremely Large Telescope (E-ELT) is already known to be Armazones, near Paranal (Chile). The selection was based on a variety of considerations, with an important one being the quality of the atmosphere for the astronomy planned for the ELT. We present an overview of the characterization of the atmospheric parameters of candidate sites, making use of standard procedures and instruments as carried out within the Framework Programme VI (FP6) of the European Union. We have achieved full characterization of the selected sites for the parameters considered. Further details on adaptive optics results and climatology will be the subject of two forthcoming articles. A summary of the results of the FP6 site-testing campaigns at the different sites is provided.

Online material: color figures

1. INTRODUCTION

In 2003 September, two major European projects were presented during the Second Backaskog Workshop on Extremely Large Telescopes in Sweden, the Euro50 (Andersen et al. 2003), a 50 m telescope developed by Lund Observatory, and the Overwhelmingly Large Telescope (OWL),[8] a 100 m telescope planned by ESO. Both projects are in competition and there has been some technical evolution. After an evaluation process,[9] the OWL was downsized to a 42 m telescope, and the new concept was presented at the SPIE conference in Marseille, France, 2008 June 23–28.[10]

Whatever the telescope concept, the site selection for the future European Extremely Large Telescope is a fundamental issue and has been undertaken within the "ELT Design Study" proposal funded by the European Union within Framework Programme 6. The first meetings and contacts to define the project started in 2003. Possible interested partners and institutions were approached and a first version with the design and plans was submitted to the European Union commission in 2004 February. After revision, using feedback from the committee, the final proposal was accepted at the end of 2004. The site characterization work package began formally in 2005 and ended in 2009 June.

The organization, working scheme, and baseline frameworks will be discussed here. For the definition of the tasks, considerable use has been made of all previous efforts that have been carried out during the past decade in the definition of techniques and reliable tools for the study of the atmosphere above astronomical sites. Our approach to site-testing is mainly based on a previous study by Vernin & Muñoz-Tuñón (1992), which in turn refers to an article by Roddier et al. (1990). Our initial philosophy was detailed by Muñoz-Tuñón et al. (2007).

[1] Université de Nice-Sophia Antipolis, Observatoire de la Côte d'Azur, CNRS-UMR6525, 06108 Nice Cedex 2, France; vernin@unice.fr, trinquetvernin@unice.fr.

[2] Instituto de Astrofísica de Canarias, c/Vía Láctea s/n, E-38205, La Laguna, Tenerife, Spain; cmt@iac.es, jdelgado@iac.es, jjf@iac.es, mreyes@iac.es, hvr@iac.es, avp@iac.es.

[3] Departamento de Astrofisica, Universidad de La Laguna E-38205, La Laguna, Tenerife, Spain.

[4] European Southern Observatory, Karl-Schwarzschild-Strasse, 2-85748 Garching bei München, Germany; msarazin@eso.org, glombard@eso.org, jnavarre@eso.org.

[5] High Energy Physics and Astrophysics Laboratory, Université Cadi Ayyad, Faculté des Sciences Semlalia, Avenue Prince My Abdellah, BP 2390, Marrakesh, Morocco; benhida@ucam.ac.ma, zouhair@ucam.ac.ma, hach-youssef@yahoo.fr, lazrek@ucam.ac.ma, sabilmohammed@yahoo.fr.

[6] Département de Physique Appliquée, Faculté des Sciences et Techniques, UCAM, BP 549, Marrakesh, Morocco.

[7] Instituto de Astronomía Teórica y Experimental, Observatorio Astronómico de la Universidad Nacional de Córdoba. Laprida 854, Córdoba, Argentina; dgl@oac.uncor.edu, pablo@oac.uncor.edu, vrenzi@oac.uncor.edu, rubenv@oac.uncor.edu.

[8] See http://www.eso.org/sci/facilities/eelt/owl/.

[9] See http://www.eso.org/sci/facilities/eelt/owl/Phase_A_Review.html.

[10] See http://www.eso.org/sci/libraries/SPIE2008/.

It is also important to highlight that studies of the atmosphere have achieved the status of key projects for the most important astronomical sites. We have therefore taken advantage of the amount of data already available that have naturally defined a ranking among known sites, which have been taken as the bottom line for preselecting potential sites.

For practical reasons, the work is divided into four tasks, ordered to better achieve our goal:

WP12000.—Site characterization and general management review, discussion, reports, and final conclusions.

WP12100.—Review of parameter space.

WP12200.—Instrumentation, measurement, and modeling.

WP12300.–Large-scale atmospheric properties.

The fourth item was introduced to assess the behavior of the wavefront at a large baseline, i.e., 100 m, which was the envisaged OWL diameter. Many articles have shown that the phase structure function increases with as $r^{5/3}$, according to Kolmogorov theory, eventually saturating at the so-called outer scale L_0, which fluctuates on the scale of meters or tens of meters. But Coulman & Vernin (1991) expected a new phase variance increase for $r \gtrsim 1200$ m; the last value is not well known and is subject to great variations. The results and experiments will be discussed elsewhere. The lidar (University of Barcelona) experiment sampling of the boundary layer has been carried out only at the Observatorio del Roque de Los Muchachos (ORM; Sicard et al. 2010).

The three main institutions involved in this project are the Université de Nice—Sophia Antipolis (UNI), the Instituto de Astrofísica de Canarias (IAC), and ESO. Marrakesh University and the Observatorio Astronómico de Córdoba (OAC) have also been involved in the working group, although their participation has been channeled through UNI and ESO.

2. SITE PRESELECTION

As a first step, we selected the sites to be investigated. To aid us in this task, we have taken into account the Thirty Meter Telescope (TMT) site-selection program, and all the TMT candidates (all situated on the American continent) have been excluded from the European search. The TMT team has already published 12 articles, one of which gives an overview of the whole site-testing campaign (Schöck et al. 2009). In Figure 1, we identify the locations of the preselected sites on a world map.

We preselected two sites, which will be considered as references: the Observatorio Roque de los Muchachos on La Palma in the Canary Islands (Spain) and Ventarrones (Chile), 40 km north of Paranal.

Two other sites were also considered as alternatives to the reference sites: Aklim in the Moroccan Anti-Atlas and Macon in northwest Argentina. A third possibility, Izaña (Observatorio del Teide [OT]) at Tenerife was considered at the very beginning and discarded due to the lack of funding afterward. Dome C in Antarctica was also considered for comparison, but not under the European Extremely Large Telescope Design Study (ELT-DS) contract. The main geographical parameters of the sites are summarized in Table 1, and their locations are shown in Figure 1.

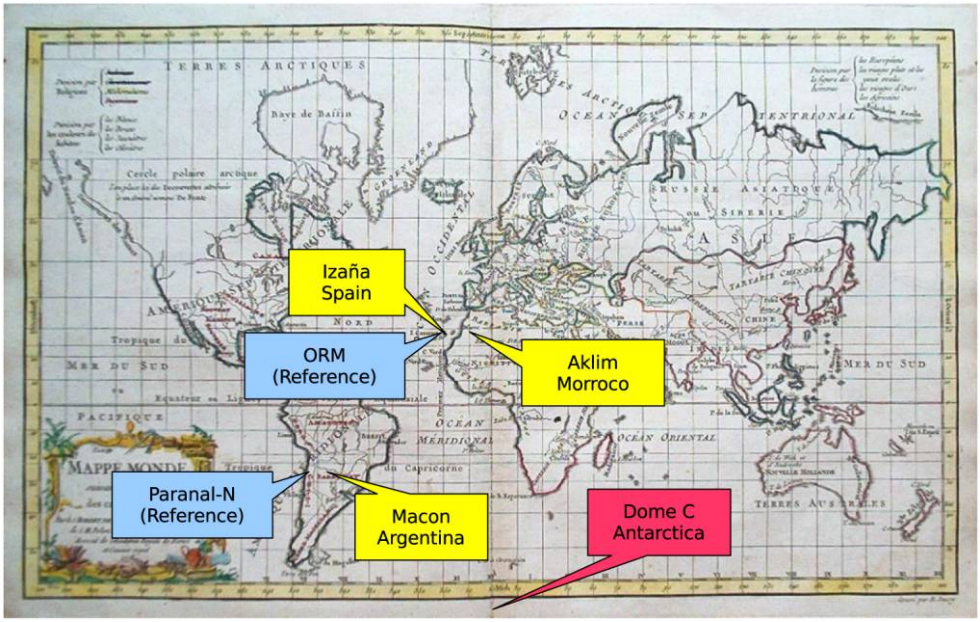

FIG. 1.—Selected sites: ORM and Paranal-N (Cerro Ventarrones, close to Paranal) have been chosen as reference sites in the northern and southern respective hemispheres, as they are recognized to be superb sites. Aklim, in the Moroccan Anti-Atlas, and Macon, in Argentina, are both considered as an alternative to their close references. See the electronic edition of the *PASP* for a color version of this figure.

TABLE 1
LATITUDE, LONGITUDE, AND ALTITUDE OF FOUR SITES BEING CHARACTERIZED

Site	Latitude	Longitude	Altitude (m)
	Northern Hemisphere		
Aklim	30 07 38 N	8 18 31 W	2350
ORM	28 45 00 N	17 53 10 W	2346
	Southern Hemisphere		
Macon	24 37 21 S	67 19 41 W	4653
Ventarrones	24 23 57 S	70 25 00 W	2837

2.1. ORM

The Canarian observatories on La Palma (ORM) and Tenerife (OT) host telescopes and instruments from over 60 scientific institutions and 19 different countries that have carried out continuous astronomical observation for over 40 years. The observatories house first-class telescopes such as the 10 m Gran Telescopio de Canarias (GTC) at the ORM and the solar Vacuum Tower Telescope at the OT. The European Solar Telescope, already at an advanced stage of design, is to be located at either the ORM or the OT.

Nocturnally, the ORM has been monitored and characterized over several decades; for a review, see Muñoz-Tuñón (2002) and Muñoz-Tuñón et al. (2007). Over 20 years' worth of data have been published, confirming the world-class astronomical characteristics of the observatories, with a stable, well-known, and predictable atmosphere. The ORM (see Fig. 2) is situated at the edge of the caldera that forms the Taburiente National Park, 2346 m above mean sea level on La Palma.

Conditions at the observatory are excellent not only for nighttime observations, but also for solar physics. The observatory also attracts researchers in high-energy astrophysics. In 1992 March, a national law was established for the protection of the astronomical quality of both the ORM and the OT. The IAC's Sky Quality Protection Unit regulates the application of the law and advises local residents on compliance with the law.

A number of meteorological and climatological features combine to produce the exceptional astronomical quality of the skies above the Canary Islands. The archipelago is located in the northern subtropical zone, i.e., close to the equator, but beyond the reach of tropical storms; the whole of the northern celestial hemisphere and a substantial part of the southern celestial hemisphere can be observed from the two astronomical sites; and the observatories are located 2400 m above mean sea level, well above the temperature inversion layer produced by the trade winds. The predominant trade winds and the cold sea current that bathes the islands result in a pleasant climate and the division of the troposphere into two distinct layers through temperature inversion, where the cloud base becomes stabilized at about 1500 m (Varela et al. 2008). The cloud layer acts as a lid, preventing atmospheric, particulate, and light pollution from contaminating the observatories. In the upper layer, the predominant winds are dry and turbulence-free and the atmosphere is extremely clear, with very low cirrus (high cloud) frequency.

2.2. Aklim

Djbel Aklim (see Fig. 3) is situated 110 km east of Agadir. At the beginning of the Moroccan site-selection process, Djbel Lekst was also foreseen as a good candidate. Both Aklim and Lekst are located in a low-risk seismic area, consisting of pre-Cambrian rock formations. Because of the tight schedule and the need to undertake the measurements, Lekst was discarded because of its lower altitude and its proximity to light pollution from Agadir. Aklim lies in a dry and desertic region with a global weather situation not far from those of the ORM region. It is clear that both areas benefit from very low annual precipitation, even when taking into account the local situation related to site altitude.

Mount Aklim is very isolated with no large city in the vicinity. There is no access road yet. A four-wheel-drive vehicle is necessary to reach the lower part of the site, followed by a 2–3 hr walk to reach the summit. Figure 3 shows part of the flat summit with enough space to accommodate large infrastructure.

It should be noted that measurements started at Aklim site using a Moroccan differential image motion monitor (DIMM) before delivery of the multi-aperture scintillation sensor (MASS)-DIMM instrument. The results of this study are summarized by Sabil et al. (2010).

2.3. Ventarrones

Cerro Ventarrones is located 35 km northeast of Paranal and 20 km north of Armazones. Armazones has been studied by the

FIG. 2.—General view of the ORM. The location of the measurements site (Degollada del Hoyo Verde) at the ORM is near the GTC (second big dome to the left). See the electronic edition of the *PASP* for a color version of this figure.

FIG. 3.—Top of the Aklim site showing that a lot of space is available for accommodating the infrastructure for a large telescope. To the left is the 5 m high MASS-DIMM tower, with the Atlas range in the background, 130 km to the north. See the electronic edition of the *PASP* for a color version of this figure.

TMT group since 2004, and a preliminary campaign conducted in 2006–2007 on the only available summit within the ESO territory (La Chira, 2559 m) had not given satisfactory results. Ventarrones was chosen based on the results of meteorological modeling of a 50×50 km area around the VLT observatory performed by the Institute for Meteorology of Munich Ludwig Maximilian University (Germany) using the PSU/NCAR MM5 mesoscale model.

The Ventarrones station started operation in 2008 January with MASS and a meteorological station (10 m). The DIMM was added in 2008 May (see Fig. 4). The station is fully robotic, with a simplified supervisor as a slave of the VLT-Paranal station: it is operated only when the Paranal DIMM is operating and observes the same targets.

2.4. Macon

The Macon station (see Fig. 5) started operation in 2008 May with a meteorological station (10 m). The MASS and DIMM were added in 2008 July. The station is remotely controlled 365 nights per year by operators lodging in the town of Tolar Grande, in direct view of the summit (altitude 3500 m). The infrastructure, logistics, and operation are funded by this work package under a dedicated contract with the Instituto de Astronomía Teórica y Experimental group of the Córdoba Observatory.

The station is located 10 km (in a straight line) from the town of Tolar Grande. The site can be accessed by 30 km of unpaved state road and 12 km of a private road built in 2007 with FP6 funds. The site has a shelter, a photovoltaic power plant of 4.5 kVA, and a 2.4 GHz radio link. The small town of Tolar Grande has lodging accommodation, cellular phone service, Internet, and a medical center. The town is located 190 km from San Antonio de los Cobres, a medium-sized city, and is 290 km distant from Salta City, capital of the province, which has international lodging facilities, an airport, health centers, and universities. After the FP6 measurement period, several studies related to the wind speed, the major drawback of the site, were performed. Hydrodynamic simulations indicated that the meteorological station used during FP6 was installed at the point with highest wind acceleration due to the combined action of the wind pattern and the sharp edge of the mountain. Subsequent measurements indicated that the wind speed decreases with increasing distance from the mountain edge. At present, a medium-sized astronomical facility is being built 150 m to the east of the FP6 measuring point.

3. PARAMETER SPACE

The costs related to the construction and maintenance of new large observatories are so high that it is necessary to optimize the use of observing time, sky transparency, and seeing conditions. In order to optimize observatory management and personnel, as well as instrument safety, one needs to know local meteorological parameters such as wind speed, temperature, and humidity.

In modern astronomy, emphasis is placed on high angular resolution techniques such as adaptive optics and interferometry. As an example, an adaptive mirror is part of the five-mirror combination of the E-ELT. Assuming a set of sites that all benefit from an equivalent number of good observing nights, it is now mandatory to study the behavior of the optical turbulence in detail: not only the integrated seeing ε, but also its distribution within the atmosphere, because this conditions other integrated parameters such as the isoplanatic angle θ_0 and the coherence time τ_0 of the wavefront. Given a seeing, the balance between ground-level and free-atmosphere turbulence has a great impact on the isoplanatic angle and the coherence time and thus on adaptive optics.

The FP6 E-ELT site-testing group selected a list of key parameters to be ideally measured at each site in accordance with the scientific and technical requirements:

Turbulence-related features.—Optical turbulence and wind speed profiles, $C_N^2(h)$ and $\mathbf{V}(h)$; integrated optical turbulence parameters: ε, θ_0, and τ_0;[11] and wind profile climatology.

Meteorological conditions.—Standard meteorological parameters (wind speed and direction, relative humidity, barometric pressure, and air temperature); precipitable water vapor; atmospheric extinction; cloud cover; and aerosols (including mineral dust).

[11] Seeing, isoplanatic angle, and wavefront coherence time, respectively.

FIG. 4.—Panorama as seen from Cerro Ventarrones. See the electronic edition of the *PASP* for a color version of this figure.

Other parameters.—Sky brightness, sodium layer, ground deformation and ground topology, seismicity, and condensation trails (from airplanes).

However, for time scheduling and practical reasons, only a set of these parameters could be measured and compared with similar instruments at each site, and these are discussed in this article. Other parameters will be analyzed and discussed in forthcoming articles.

4. APPROPRIATE INSTRUMENTATION

At the outset, it was decided to use the same standard instruments in the four selected sites. But it soon became apparent that, for example, the construction of five fully robotized MASS-DIMM instruments was impossible within our budget. In this case, we decided to build two MASS-DIMM versions: robotized (no human intervention) and automated (human intervention, but with automatic tracking). In both cases, the telescope and the focal instruments are the same, with different mounts and different interaction (supervisor) with the environment (weather). The implication is that, in remote areas, considerable manpower is necessary to run automated instruments.

For financial reasons, after FP6 negotiation, it was no longer possible to fulfill all these expectations, and we downsized our ambitions to the instruments listed in Table 2. It was decided to use a more advanced version of the generalized scintillation detection and ranging (SCIDAR) called the "cute-SCIDAR." The single-star SCIDAR was studied, constructed, and installed at Nice Observatory, but because of its price, it was impossible to install an instrument for each site. The Argentinian MASS-DIMM was robotized with extra FP6 ESO funds. Robust image processing software for the All-Sky Camera was not available, and it was decided to withdraw this instrument from this project. No boundary-layer profiler was available.

Satellite data were also used to monitor aerosol content and cloud cover (Varela et al. 2008).

4.1. DIMM

The differential image motion monitor (Stock & Keller 1960; Sarazin & Roddier 1990; Vernin & Muñoz-Tuñón 1995) operates by measuring the wavefront slope differences over two small pupils some distance apart. Because it is a differential method, the technique is inherently insensitive to telescope tracking errors. This method is implemented with a 28 cm aperture telescope and a fast-readout CCD. A set of a few hundred exposures of 5–10 ms allows a single measurement of the integrated seeing. When observing a star, the images coming from the aforementioned two pupils are observed with the CCD. Their centroids are determined from the whole set of 200 or 400 exposures. The variances of the longitudinal and transverse differential motions σ_l and σ_t are both related to the integrated seeing $\varepsilon_{\rm DIMM}$. In order to avoid the surface-layer contribution, all our DIMMs were installed on 5 m platforms.

DIMM seeing measurements are affected by different sources of bias such as image threshold, defocus, exposure time, photon noise, and high-frequency vibrations that must be monitored in real time and that led us to reject part of the measurements. The outer scale of optical turbulence might also induce some seeing error (Berdja 2010). Nevertheless, since the outer scale does not vary very much from one site to another, a DIMM, once it has been well calibrated, may be considered a very reliable and quantitative monitor. The DIMMs were cross-calibrated, taking simultaneous measurements, with the IAC DIMM at the ORM during several nights. The instruments were in very good agreement (ELT/MASS_DIMM calibration at ORM.[12] Details will be presented in the future article on high angular resolution (Paper II).

4.2. MASS

This instrument detects rapid variations of light intensity in four concentric apertures using photomultipliers. The 1 ms photon counts accumulated during 1 minute are converted to four normal scintillation indices and to six differential indices for each pair of apertures. This set of 10 numbers is fitted by a model of six thin turbulent layers at predefined altitudes of 0.5, 1, 2, 4, 8, and 16 km above the site (see Kornilov et al. 2003). Another model of three layers at "floating" altitudes is fitted as well. Raw measurements are filtered according to criteria such as low flux and misalignment (Kornilov et al. 2007).

Turbulence near the ground does not produce any scintillation: MASS is "blind" to it and can only measure the seeing in the free atmosphere, $\varepsilon_{\rm MASS} = \varepsilon_{\rm FA}$. MASS has been cross-compared with

[12] See http://www.iac.es/site-testing/images/stories/publication/complementarynote.pdf

FIG. 5.—Macon range as seen from the bottom salar. See the electronic edition of the *PASP* for a color version of this figure.

the G-SCIDAR during a campaign performed at Mauna Kea (Tokovinin et al. 2005).

The MASS and DIMM observe simultaneously in order to give access to the boundary-layer contribution:

$$\varepsilon_{\rm BL} = (\varepsilon_{\rm DIMM}^{5/3} - \varepsilon_{\rm MASS}^{5/3})^{3/5}. \quad (1)$$

Due to noise in the seeing measurement, it might happen that $\varepsilon_{\rm DIMM} < \varepsilon_{\rm MASS}$. In this case, both measurements are rejected. Note that it only happens when DIMM and MASS seeing are similar, that is, when the ground layer is weak. Thus, by using this approach we preferentially exclude data with a weak ground layer. However, this will be discussed in Paper II.

5. THE SCIDAR FAMILY

SCIDAR is based on the multidimensional analysis of stellar scintillation, i.e., the flux that reaches the ground after crossing the turbulent atmosphere. The SCIDAR principle is illustrated in Figure 6. This flux is a function of the position of the observer, time, the direction toward the star, and the wavelength $I(x, y, t, \alpha, \beta, \lambda)$. SCIDAR analyzes this flux, which is spread over the entrance pupil of a telescope. Cute-SCIDAR (an automated version of the generalized SCIDAR [see Vázquez Ramió et al. 2008]) computes the spatioangular auto- and cross-correlations on a projection along the x, y, α, β, and t axes. Single-star SCIDAR (SSS; Habib et al. 2006) computes the spatiotemporal auto-and cross-correlation on a projection along the x, y, and t axes. Cute-SCIDAR and SSS allow us to retrieve both the C_N^2 and **V** vertical profiles.

TABLE 2

INSTRUMENTS INSTALLED AT THEIR CORRESPONDING SITES

	ORM	Ventarrones	Aklim	Macon
Cute-SCIDAR	Y	Y	N	N
SSS	N	N	N	N
MASS/DIMM	Y	Y	Y	Y
$\mathcal{R}$-mount	N	Y	N	Y (ESO)
$\mathcal{A}$-mount	Y	N	Y	N
All-sky camera	N	N	N	N
High-alt. dust	Y	N	Y	Y
AWS	Y (IAC)	Y (ESO)	Y (UNI)	Y (ESO)
BL profiler[a]	N	N	N	N
Climat. sat.	Y	Y	Y	Y
Meteo. model	Y	Y	Y	Y

[a] BL profiler might be an optical turbulence profiler within the boundary layer, not yet available.

5.1. Cute-SCIDAR

Cute-SCIDAR is a fully automated instrument, meaning complete control of the displacement of the optical elements, positioning of the conjugate plane (OZ axis), centering in the (X, Y) plane, and rotation of the whole system to adjust the direction of the pixel grid to the observed binary star alignment. These motions are controlled from a user-friendly graphical interface. The most recent improvement of cute-SCIDAR is a custom-made software package performing fast data acquisition and processing, which can give the turbulence profiles in real time, with and without any turbulence contribution from the dome. As a consequence, alignment and observation procedures reduce to easy handling without the need of an operator in the dome.

5.2. Single-Star SCIDAR

Due to the additional costs and lack of feasibility tests, the development work on the SSS technique was carried out with future site-testing in mind, rather than its immediate use within this FP6 project. During this period, we constructed a prototype and observed at Nice Observatory, carefully verifying that this instrument was delivering quantitative measurements of both the $C_N^2(h)$ and $\mathbf{V}(h)$ profiles. The SSS is also running at Dome

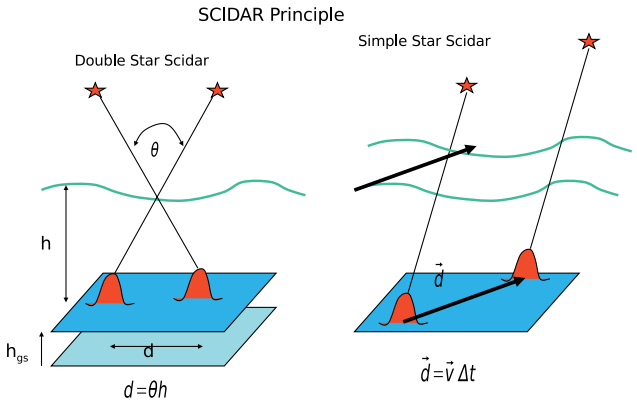

FIG. 6.—Principle of both generalized and single-star SCIDARs. See the electronic edition of the *PASP* for a color version of this figure.

C, Antarctica, and has been carefully compared with simultaneous DIMM measurements (Vernin et al. 2009).

5.3. Automated Weather Station

Various types of automated weather stations (AWSs) have been used for the E-ELT site characterization campaign at the ORM (Casella), Ventarrones (Vaisala), Macon (Vaisala), and Aklim (La Crosse Technology). The ORM site hosts other AWSs operated by the different institutions. Data are publicly accessible. The AWS delivers wind speed and direction, pressure, temperature, and humidity. All AWS wind speed sensors have been placed at 10 m above ground, except at Aklim, where wind measurements are recorded at 2 m. Pressure, temperature, and humidity sensors have been situated 2 m above ground at the ORM and Aklim and at 10 m at Ventarrones and Macon.

6. OBSERVATION AND DATA REDUCTION

In order to avoid possible measurement distortion between the four sites, the instruments were almost identical (see § 4). Observing periods were determined in advance, and the criteria of data rejection were homogeneous. All the data (MASS, DIMM, and AWS) coming from the four sites were regularly uploaded, month after month, to a special archive at the IAC. Data processing was discussed and agreed upon between all the participants and implemented in IDL software within an IAC server. All the data, as well as rejection filters and data processing software, were accessible to all the participants. In Figure 7, the temporal coverage of the DIMM/MASS instrument throughout 2008 and 2009 is sketched. Routine measurements began in 2008 April and ended in 2009 June, at the end of the FP6 contract, except for Aklim and the ORM, which continued to observe. As mentioned before, the density of measurements made with robotic instruments is greater than that of automatic ones.

7. OVERVIEW OF THE RESULTS

7.1. Fraction of Clear Sky

The fraction of clear sky and related parameters (useful observing time) are vital for astronomical site selection. Cloud cover can be determined using either ground-based techniques (all-sky-cameras, cloud radar, infrared radiometers, etc.) and observer assessment recorded at many ground telescopes or through satellite measurements.

Satellites have the advantage of providing a long-term (longer than 5 yr) database for many sites in the world by using comparable spectrographs and techniques. Nevertheless, the agreement between in situ and satellite measurements depends strongly on the spatial resolution (Kurlandczyk & Sarazin 2007; Varela et al. 2008) and on the scanning geolocation. Astronomical observatories are often located on high mountains, and terrain can change very rapidly. Therefore, very high nighttime spatial resolution satellite data are to be recommended for astronomical site characterization. In particular, high vertical resolution and the use of appropriate channels to detect different types and levels of clouds make the satellite data a useful tool for clear/photometric time characterization for astronomical observations.

The clear fraction of sky has been the subject of study of Erasmus & van Rooyen (2006) for quite a large number of years. As result, they have carried out specific studies for determining the useful time for a large number of regions of the world, making use of satellites and defining very precisely the technique for suitable data interpretation. Erasmus et al.'s reports have been promoted and purchased from different institutions. The following is a summary of the results obtained at Paranal (Chile), at the ORM (La Palma, Spain), and at Aklim (Morocco).

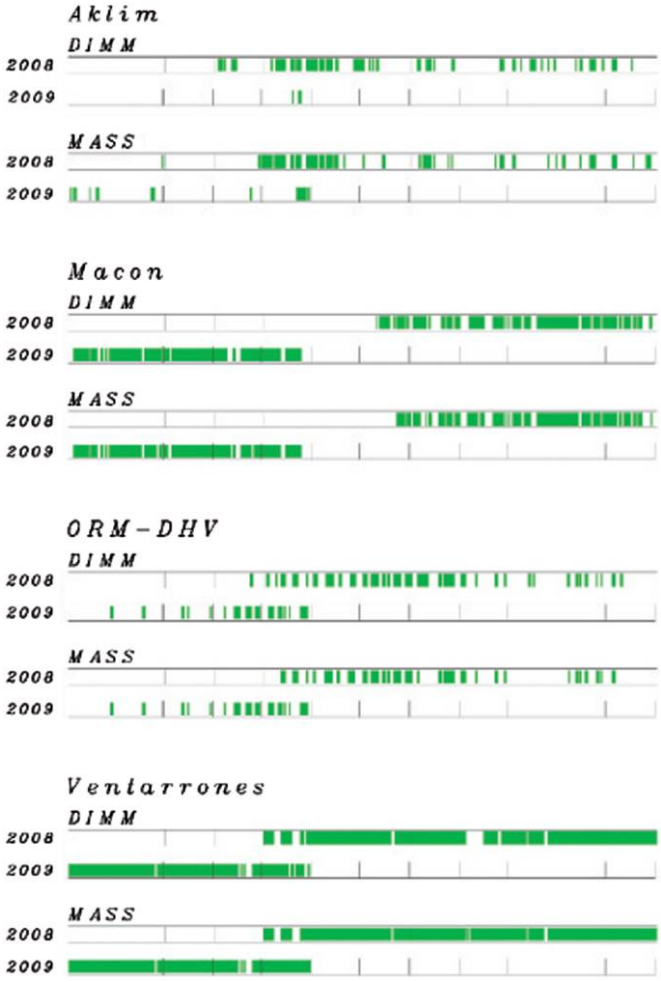

FIG. 7.—Observing time coverage of each site and instrument (MASS and DIMM). Each year is divided into months by lines. The Macon and Ventarrones sites implemented robotic systems, while the Aklim and ORM site observations are carried out by observers. See the electronic edition of the *PASP* for a color version of this figure.

7.1.1. Results at Paranal

The satellite survey of cloud cover and water vapor in Northern Chile by Erasmus & Maartens (2001) was conducted for CTIO and the University of Tokyo using satellite data from the International Satellite Cloud Climatology Project (ISCCP) data set: Meteosat-3 (1993–1994) and GOES-8 (Geostationary Operational Environmental Satellite 8; 1995–1999). The spatial resolution was 9.1 km × 8.0 km, and the temporal resolution was 3 hr. The bands used were 6.7 μm (water vapor) and 10.7 μm (IR window). They conclude that 84.6% of the nights are photometric (or "clear") at Paranal, cross-calibrated at ground level with LOSSAM (Line-of-Sight Sky Absorption Monitor), which provides a clear fraction verified to be accurate to within 1%.

7.1.2. Results at ORM

From the satellite survey of cloud cover and water vapor in Morocco and Southern Spain and verification using La Palma ground-based observatories (Erasmus & van Rooyen 2006) was conducted by ESO using EUMETSAT (European Organization for the International Exploitation of Meteorological Satellites)-ISCCP data over a period of 7 yr (1996–2002). The spatial resolution was 5 km × 5 km, and the temporal resolution was 3 hr. Data channels used for this analysis were 6.4 μm (water vapor) and 11.5 μm (IR) for cloud cover in the middle/upper troposphere and precipitable water vapor.

Erasmus & van Rooyen (2006) conclude that the photometric (also called "clear") observing time at the ORM is 83.7%. Cross-calibration at ground level with the atmospheric extinction coefficient in $V(K_V)$ provided by the Carlsberg Meridian Telescope was verified to be accurate within 1.2%. This result is in agreement with the global estimate of 20.7% of weather downtime by Garcı´a-Gil et al. (2010) for the period 1999–2003, based on the log of the Carlsberg Meridian Telescope.

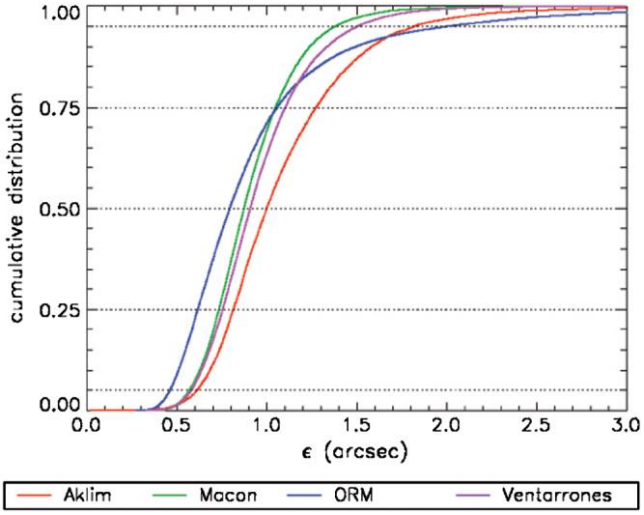

FIG. 8.—Cumulative distribution of seeing values at the Aklim, ORM, Macon, and Ventarrones sites. See the electronic edition of the *PASP* for a color version of this figure.

A recent study using nighttime GOES12 in 2007–2008, provides 88% and 72.5% of clear time at Paranal and La Palma, respectively (Cavazzani et al. 2011). The difference with Erasmus & van Rooyen (2006) is understood by Cavazzani et al.'s (2011) shorter sampling period (2 yr). Moreover, Erasmus & van Rooyen (2006) use a sampling area that fixes better with the ORM site. This is less important in the orography of Paranal.

7.1.3. Results at Aklim

Erasmus & van Rooyen (2006) show the map of the distribution of clear skies for nighttime over a 7 yr period (1996–2002) covering Morocco. The clearest locations in the Atlas Mountains are those located furthest south and west, i.e., in the Anti-Atlas. At the Aklim geolocation the clear time is 76%.

TABLE 3
GLOBAL MEDIAN VALUES OBTAINED DURING ELT-DS PERIOD

Parameter	Instrument	Aklim	ORM	Ventarrones	Macon
Total seeing ε (″)	DIMM	1.00	0.80	0.91	0.87
Isoplanatic angle θ_0 (″)	MASS	1.29	1.93	1.96	1.37
Coherence time τ_0 (ms)	MASS/DIMM/NOAA	3.53	5.58	4.90	3.37
Optical étendue G_0 (m^2 ms $arcsec^2$)	MASS/DIMM/NOAA	0.05	0.38	0.26	0.10
Free-atmosphere seeing (″) ε_{FA}	MASS	0.52	0.31	0.55	0.66
Boundary-layer seeing (″) ε_{BL}	DIMM-MASS	0.77	0.65	0.60	0.51
Cloud: clear fraction (%)	Satellite	76	84	85	75
Night temperature at 2 m (°C)	AWS	12.5	7.3	10.9	−0.2
Night relative humidity at 2 m (%)	AWS	32	21	14	20
Night wind speed at 10 m (m/s)	AWS	6.2[a]	8.2	5.9	11.3
Night pressure at 2 m	AWS	767.0	772.4	727.0	581.8

[a] At Aklim, night wind speed was measured at 2 m.

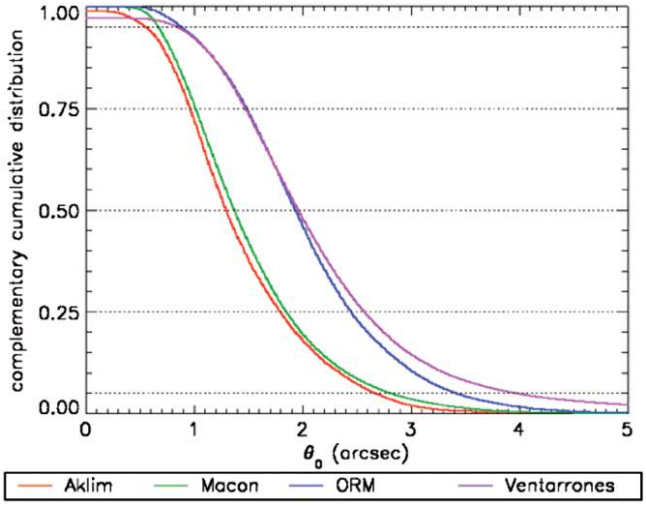

FIG. 9.—Complementary cumulative distribution of isoplanatic-angle values at the Aklim, ORM, Macon, and Ventarrones sites. See the electronic edition of the *PASP* for a color version of this figure.

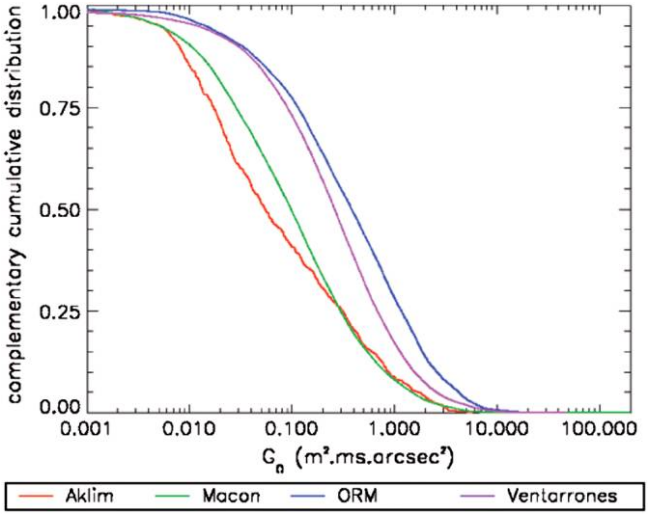

FIG. 11.—Complementary cumulative distribution of optical étendue values at the Aklim, ORM, Macon, and Ventarrones sites. See the electronic edition of the *PASP* for a color version of this figure.

7.1.4. Results at Macon

At the geographical coordinates of Macon for the period of 1993–1999, Erasmus & Maartens (2001) provide a percentage of 75% for clear nighttime, 20% opaque, and 5% partially cloudy and transparent cirrus.

7.2. High Angular Resolution Astronomy

The major parameters relevant to high angular resolution (imaging, adaptive optics, and spectroscopy) have been sorted into two classes: integrated parameters and profiles. The latter class is represented by optical turbulence profiles $C_N^2(h)$ and wind velocity profiles $\mathbf{V}(h)$. It is well known that integrated parameters such as seeing or Fried's radius, isoplanatic angle,

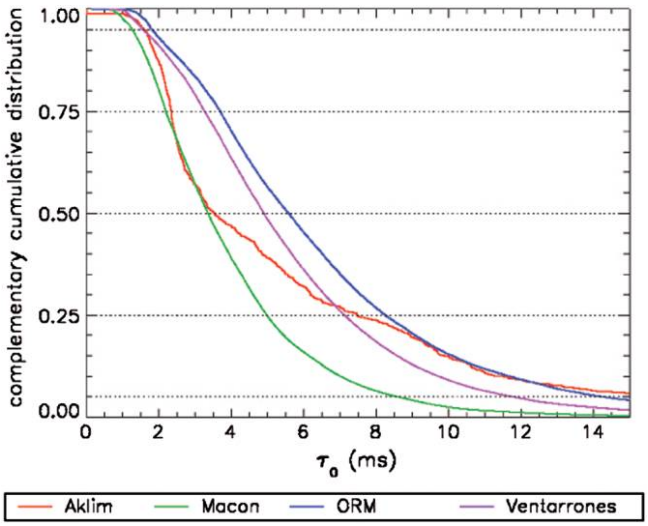

FIG. 10.—Complementary cumulative distribution of coherence time values at the Aklim, ORM, Macon, and Ventarrones sites. See the electronic edition of the *PASP* for a color version of this figure.

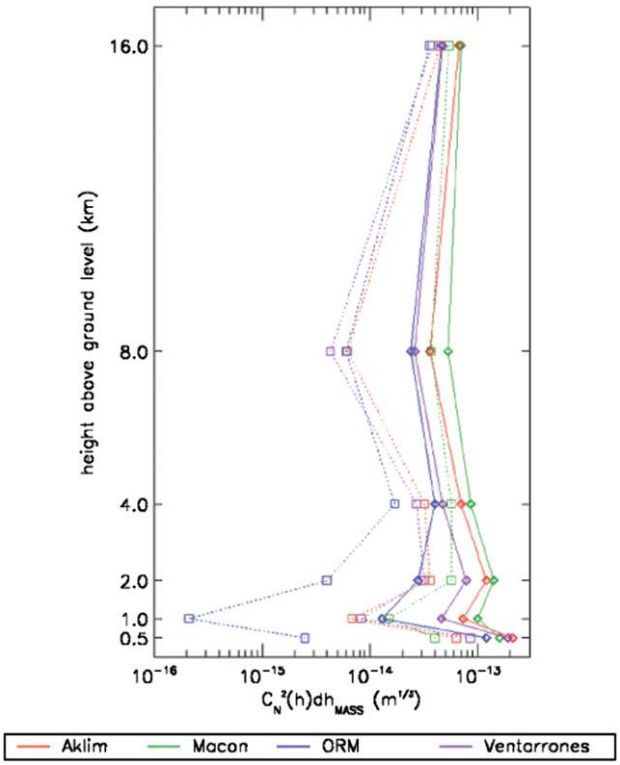

FIG. 12.—Mean (*diamonds/solid line*) and median (*squares/dashed line*) $C_N^2(h)dh$ values corresponding to the whole campaign (until 2009 May) obtained at the Aklim, Macon, ORM, and Ventarrones sites. See the electronic edition of the *PASP* for a color version of this figure.

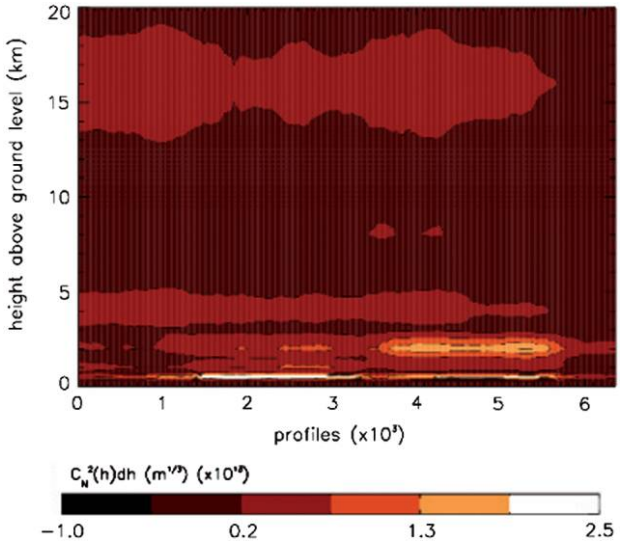

FIG. 13.—Optical turbulence profiles measured by the MASS instrument at the Aklim site during the whole campaign (until 2009 May). Contour levels are labeled at the bottom. See the electronic edition of the *PASP* for a color version of this figure.

and coherence time can be deduced from both of the previous profiles:

Fried's radius is

$$r_0 = 0.185\lambda^{6/5}\left(\int_0^\infty C_N^2(h)dh\right)^{-3/5}. \quad (2)$$

Seeing is

$$\varepsilon_{\rm fwhm} = 0.98\frac{\lambda}{r_0} = 5.25\lambda^{-1/5}\left(\int_0^\infty C_N^2(h)dh\right)^{\frac{3}{5}}. \quad (3)$$

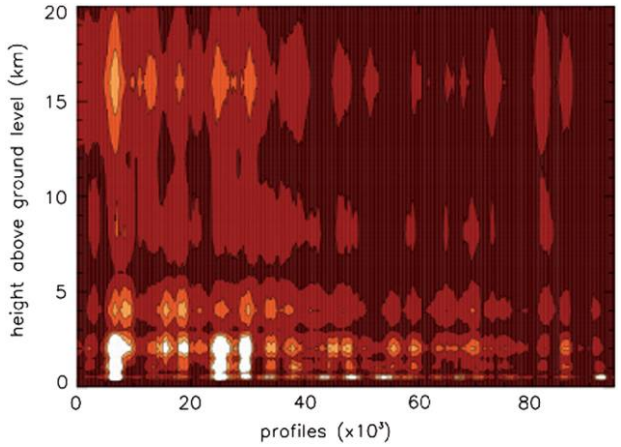

FIG. 14.—Optical turbulence profiles measured by the MASS instrument at the Macon site during the whole campaign (until 2009 May). Contour levels are labeled at the bottom of Fig. 13. See the electronic edition of the *PASP* for a color version of this figure.

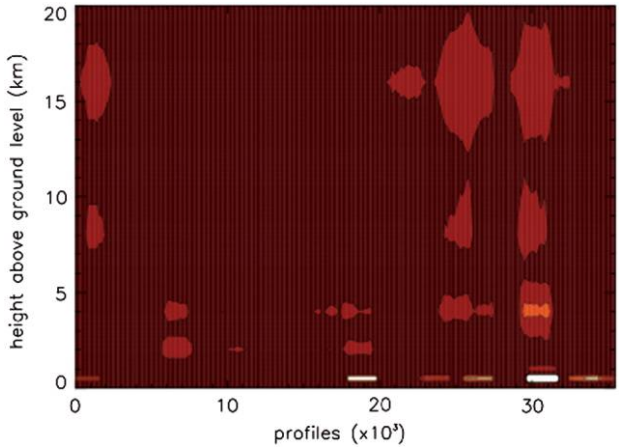

FIG. 15.—Optical turbulence profiles measured by the MASS instrument at the ORM site during the whole campaign (until 2009 May). Contour levels are labeled at the bottom of Fig. 13. See the electronic edition of the *PASP* for a color version of this figure.

Isoplanatic angle is

$$\theta_0 = 0.058\lambda^{6/5}\left(\int_0^\infty h^{5/3}C_N^2(h)dh\right)^{-3/5}. \quad (4)$$

Coherence time is

$$\tau_0 = 0.058\lambda^{6/5}\left(\int_0^\infty |\mathbf{V}(h)|^{5/3}C_N^2(h)dh\right)^{-3/5}. \quad (5)$$

where the light wavelength is $\lambda = 0.5$ μm in this study and all the measurements were corrected from the line of path to the zenith angle.

In various areas of astronomical technique, authors propose different relationships between limiting detectable flux and

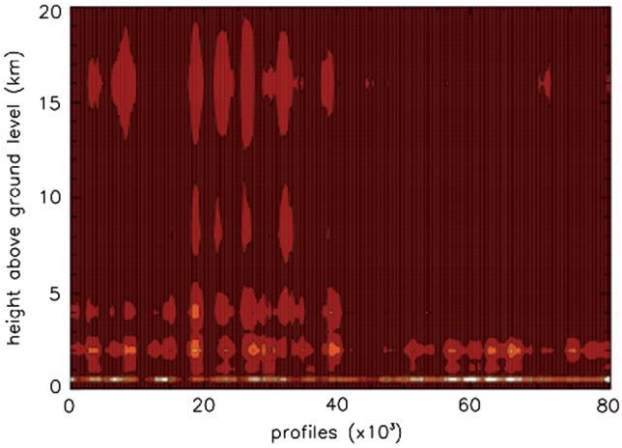

FIG. 16.—Optical turbulence profiles measured by the MASS instrument at the Ventarrones site during the whole campaign (until 2009 May). Contour levels are labeled at the bottom of Fig. 13. See the electronic edition of the *PASP* for a color version of this figure.

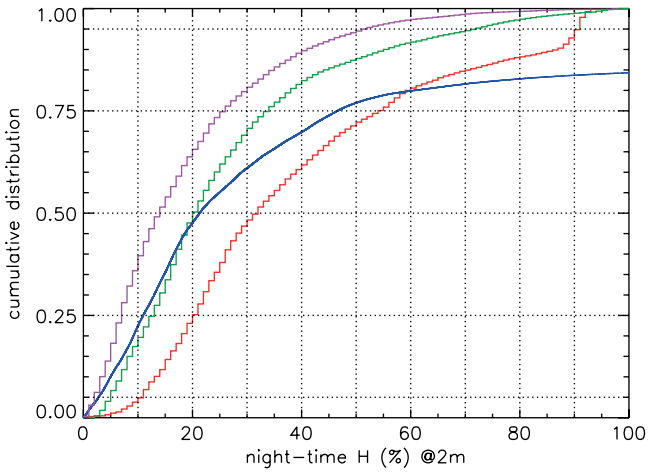

FIG. 17.—Cumulative distribution of the nighttime relative humidity at the Aklim, Macon, ORM, and Ventarrones sites. Color code is as in Fig. 8. See the electronic edition of the *PASP* for a color version of this figure.

these parameters. For spectroscopy, Dennefeld & Fort (1986) expressed this limiting flux according to

$$\Phi_{\rm lim} \propto \varepsilon/D, \tag{6}$$

where D is the telescope diameter. For high-resolution imaging, di Serego Alighieri (1986) went to the same equation (6). In speckle interferometry and according to various instrumental combinations, one finds the following relationship in the literature:

$$\Phi_{\rm lim} \propto \varepsilon^n/D^m \qquad 2 \le n \le 4 \qquad 0 \le m \le 1, \tag{7}$$

which shows the importance of seeing versus the diameter of the telescope.

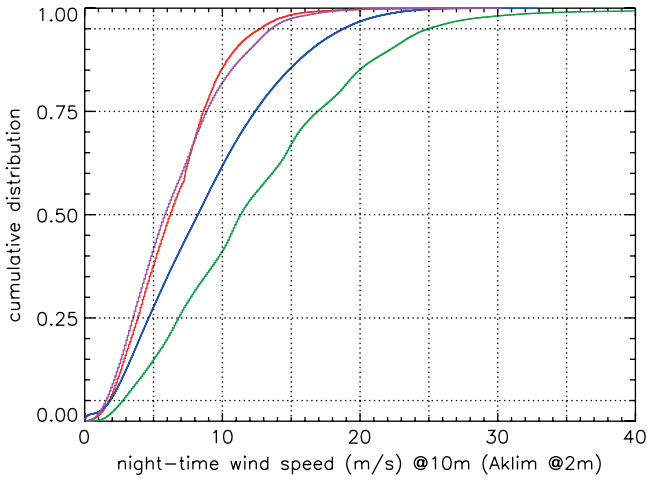

FIG. 18.—Cumulative distribution of the nighttime wind speed at the Aklim, Macon, ORM, and Ventarrones sites. Color code is as in Fig. 8. See the electronic edition of the *PASP* for a color version of this figure.

A more general approach is given by Lloyd (2004), who defines the "optical étendue" G_0 in which a photon remains coherent and which takes into account a combination of Fried's radius, isoplanatic angle, and coherence time:

$$G_0 = r_0^2 \tau_0 \theta_0^2. \tag{8}$$

This new formulation shows a strong dependence of G_0 on r_0 and θ_0. G_0 is computed with r_0, τ_0, and θ_0, respectively, expressed in m^2, $m\,s^2$, and $arcsec^2$.

Seeing.—Figure 8 gives our statistical analysis of the seeing. Global median seeing values are indicated in Table 3 and more details will appear in Paper II. The total atmosphere seeing, ε, is directly provided by the DIMM. Similarly, the free-atmosphere seeing ($\varepsilon_{\rm FA}$) and the turbulence profile ($C_N^2(h)$), 500 m above ground level are estimated with the MASS instrument. The boundary-layer seeing ($\varepsilon_{\rm BL}$) defined here as the integrated turbulence from $h = 5$ m and $h = 500$ m is evaluated from combined MASS-DIMM observations (see eq. [1]).

Isoplanatic angle.—Figure 9 gives our statistical analysis of the isoplanatic angle. Global median isoplanatic angle at each site is indicated in Table 3 and more details will be provided in Paper II.

Coherence time of the wavefront.—Figure 10 gives our statistical analysis of the coherence time of the wavefront. As expressed in equation (5), one needs to know the wind velocity profile $\mathbf{V}(h)$, as well as the $C_N^2(h)$ profile, from ground level to infinity, which cannot be derived from MASS, since it is not sensitive to ground-layer turbulence. Schöck et al. (2009) and Travouillon et al. (2009) combined $\tau_{\rm MASS}$ multiplied by a calibrating factor and the boundary-layer seeing deduced from DIMM-MASS, as expressed in equation (1), weighted by an extrapolated wind speed at a height of 40 m. We preferred a simpler method, using a full vertical profile of the C_N^2 deduced from MASS and DIMM-MASS and a wind speed vertical profile extrapolated from the NOAA Air Research Laboratory Global Data Assimilation System, with a 1° grid resolution and a 3 hr time resolution. Ground-level wind speed is measured by the local AWS. Since GDAS profiles are available every 3 hr, C_n^2 profiles from the MASS/DIMM are averaged over 3 hr around the GDAS reanalysis.

Optical étendue.—Figure 11 gives our statistical analysis of the optical étendue.

Optical turbulence profiles from MASS.—The MASS instrument measures at six different heights above ground level: 0.5, 1, 2, 4, 8, and 16 km. In Figure 12 the mean and median values obtained at each site are plotted. All the profiles measured at each of the four sites are plotted in Figures 13, 14, 15, 16 using filled contour levels.

7.3. Meteorology

Here, we present the statistical analysis of the meteorological parameters recorded. More extended information on the instrumentation, data acquisition, and analysis will be presented in

Paper III. Measurements are obtained with the AWS equipped with standard meteorological sensors providing air temperature, wind speed and direction, humidity, and barometric pressure. The statistical analysis of the data set is made separating day- and nighttime data. Day/night separation was achieved by taking the nautical twilight (Sun 12° below the horizon). As an example, we present details of the statistical distribution of the relative humidity and wind velocity. Figure 17 gives the cumulative distribution of the nighttime relative humidity. Figure 18 gives the cumulative distribution of the nighttime wind speed. Statistical results are summarized in Table 3.

8. SUMMARY

Within the framework of the installation of the future European ELT, site characterization is among the top-level requirements to ensure the best scientific return on investment. It has been made possible with the help of the European Community within the ELT Design Study project. More than five years were devoted to determining the site requirements, the first selection of the best potential sites, the selection of the instruments best fitting our goals, the construction and setting up of the monitors on each candidate site, and the synthesis of all the measurements.

Excluding the sites already selected for the TMT project, four sites were investigated, two each in the northern and southern hemispheres, using Paranal and the ORM as references and extending the potential area to the Moroccan Anti-Atlas and Argentina. Climatology and high angular resolution parameters (seeing, isoplanatic angle, and coherence time) were obtained during almost two years, with equivalent instrumentation and measurement procedures.

The summary of the results of the FP6 site-testing campaigns at the different sites is provided in Table 3. The first six rows show the global median values of seeing, isoplanatic angle, and coherence time of the wavefront, optical étendue, Fried's parameter, free-atmosphere seeing, and boundary-layer seeing, obtained during the ELT-DS period (see Fig. 7). The seventh row shows the cloud clear fraction as deduced from satellites, and the last items, at the bottom, show nighttime median values of air temperature, relative humidity, wind speed, and barometric pressure in the Aklim, Macon, ORM, and Ventarrones sites.

The final process of site selection is complex and cannot be based on one particular parameter, but on a combination of many variables, weighted by factors that depend on what kind of astronomical technique is best suited to scrutinizing the skies. Some differences are noticeable from site to site in Table 3, but in many respects these sites compare well with TMT sites, as they appear in Table 2 of Schöck et al. (2009).

We acknowledge the European Community, which granted this Extremely Large Telescope Design Study in Framework Programme 6 (contract 11863). We thank R. Gilmozzi, Principal Investigator of the European Extremely Large Telescope project, for his help and the ESO members who participated in the organization of many international meetings. We are grateful to P. Bonet, S. Rueda, and J. Rojas; to the technicians in telescope operations; and to many of the technicians of the Instituto de Astrofísica de Canarias for performing the observations and for their technical support at the Observatorio del Roque de Los Muchachos. Our acknowledgments also go to the observers at Paranal for their help and observations during the cute-SCIDAR (scintillation detection and ranging) campaigns. The Moroccan team is grateful to the Moroccan Hassan II Academy of Science and Technology, which financially supported the site-testing campaigns at the Aklim site. Our sincere gratitude also goes to the site surveyors and to all the staff members for their help and dedication: in particular, A. Habib, A. Jabiri, A. Bounhir, and the 3AM staff. We also acknowledge Hernan Muriel, Diego Ferreiro, Federico Staszyzyn, and José Viramonte for their help at Macon. We are indebted to the NOAA Air Research Laboratory administration, which supplies free meteorological archives that helped us to compute some of the parameters included in this study. We are grateful to our anonymous referee for comments and suggestions that have contributed to improving the article. Thanks to Terry Mahoney and Campbell Warden for English corrections.

REFERENCES

Andersen, T., Ardeberg, A., & Owner-Petersen, M., eds. 2003, Euro50: Design Study of a 50 m Adaptive Optics Telescope (Lund: Lund Obs.), http://www.astro.lu.se/~torben/euro50/publications/white_book80.pdf

Berdja, A. 2010, MNRAS, 409, 722

Cavazzani, S., Ortolani, S., Zitelli, V., & Maruccia, Y. 2011, MNRAS, 411, 1271

Coulman, C. E., & Vernin, J. 1991, Appl. Opt., 30, 118

Dennefeld, M., & Fort, B. 1986, in 2nd Workshop on ESO's Very Large Telescope, ed. S. D'Odorico, & J.-P. Swings (Garching: ESO), 24, 151

di Serego Alighieri, S. 1986, in 2nd Workshop on ESO's Very Large Telescope, ed. S. D'Odorico, & J.-P. Swings (Garching: ESO), 24, 173

Erasmus, D., & Maartens, D. 2001, . Final Report to ESO 2001 (58311/ODG/99/8362/GWI/LET; Garching: ESO), http://www.eso.org/gen-fac/pubs/astclim/forecast/erasmus/Reports/Erasmus-ESO-Paranal-30JUN01.pdf

Erasmus, D., & van Rooyen, R. 2006, Final Report to ESO 2006 (73526/TSD/04/6179/GW/LET; Garching: ESO), http://www.eso.org/gen-fac/pubs/astclim/forecast/erasmus/Reports/Erasmus-ESO-NWAfrica-14Feb06.pdf

García-Gil, A., Mũnoz-Tũnón, C., & Varela, A. M. 2010, PASP, 122, 1109

Habib, A., Vernin, J., Benkhaldoun, Z., & Lanteri, H. 2006, MNRAS, 368, 1456

Kornilov, V., Tokovinin, A., Shatsky, N., et al. 2007, MNRAS, 382, 1268
Kornilov, V., Tokovinin, A. A., Vozyakova, O., et al. 2003, Proc. SPIE, 4839, 837
Kurlandczyk, H., & Sarazin, M. 2007, Proc. SPIE, 6745, 674507
Lloyd, J. P. 2004, Proc. SPIE, 5491, 190
Mũnoz-Tuñón, C. 2002, in ASP Conf. Ser. 266, Astronomical Site Evaluation in the Visible and Radio Range, ed. J. Vernin, Z. Benkhaldoun, & C. Muñoz-Tuñón (San Francisco: ASP), 498
Mũnoz-Tũnón, C., Sarazin, M., & Vernin, J. 2007, in Rev. Mex. AA Ser. Conf. 31, 1
Roddier, F., Cowie, L., Graves, J., et al. 1990, Proc. SPIE, 1236, 485
Sabil, M., Benkhaldoun, Z., Lazrek, M., et al. 2010, A&A, 522, A69
Sarazin, M., & Roddier, F. 1990, A&A, 227, 294
Schöck, M., Els, S., Riddle, R., et al. 2009, PASP, 121, 384
Sicard, M., Reba, M. N. M., Tomás, S., et al. 2010, MNRAS, 405, 129
Stock, J., & Keller, G. 1960, in Stars and Stellar Systems, ed. G.P. Kuiper, & B. M. Middlehurst (Chicago: Chicago Univ. Press), 1, 138
Tokovinin, A., Vernin, J., Ziad, A., & Chun, M. 2005, PASP, 117, 395
Travouillon, T., Els, S., Riddle, R. L., Schöck, M., & Skidmore, W. 2009, PASP, 121, 787
Varela, A. M., Bertolin, C., Mũnoz-Tũnón, C., Ortolani, S., & Fuensalida, J. J. 2008, MNRAS, 391, 507
Vázquez Ramió, H., Delgado, J. M., Reyes, M., et al. 2008, Proc. SPIE, 7012, 701245
Vernin, J., Chadid, M., Aristidi, E., et al. 2009, A&A, 500, 1271
Vernin, J., & Mũnoz-Tũnón, C. 1992, A&A, 257, 811
———. 1995, PASP, 107, 265